

# How chiral forces shape neutron-rich Ne and Mg nuclei

A. Ekström,<sup>1</sup> C. Forssén,<sup>1</sup> G. Hagen,<sup>2,3</sup> G. R. Jansen,<sup>4,2</sup> T. Papenbrock,<sup>3,2</sup> and Z. H. Sun<sup>2</sup>

<sup>1</sup>*Department of Physics, Chalmers University of Technology, SE-412 96 Göteborg, Sweden*

<sup>2</sup>*Physics Division, Oak Ridge National Laboratory, Oak Ridge, Tennessee 37831, USA*

<sup>3</sup>*Department of Physics and Astronomy, University of Tennessee, Knoxville, Tennessee 37996, USA*

<sup>4</sup>*National Center for Computational Sciences, Oak Ridge National Laboratory, Oak Ridge, TN 37831, USA*

We compute the structure of the exotic even nuclei  $^{20-34}\text{Ne}$  and  $^{34-40}\text{Mg}$  using interactions from chiral effective field theory (EFT). Our results for the ground-state rotational bands in  $^{20-32}\text{Ne}$  and  $^{36-40}\text{Mg}$  agree with data. We predict a well-deformed  $^{34}\text{Ne}$  and find that  $^{40}\text{Mg}$  exhibits an oblate deformed band close to the prolate ground-state, indicating the emergence of shape co-existence at the neutron dripline. A global sensitivity analysis shows that the subleading singlet  $S$ -wave contact and a pion-nucleon coupling strongly impact deformation in chiral EFT.

*Introduction.*— Neutron-rich nuclei beyond the magic neutron number  $N = 20$  are interesting because of the breakdown of this shell closure and the interplay between nuclear deformation and weak binding in the so-called island of inversion [1–9]. In neon (proton number  $Z = 10$ ) the dripline nucleus is  $^{34}\text{Ne}$  [10, 11], and signatures of rigid rotation (with relatively low-lying  $J^\pi = 2^+$  states whose energies decrease with increasing  $N$ ) are found for isotopes with  $N = 20, 22$  [12–15]. In magnesium ( $Z = 12$ ) shape co-existence [16–18] has been observed in  $^{32}\text{Mg}$  [19], the dripline is thought to be beyond  $N = 28$ , and nuclei are deformed for  $N \geq 20$  [20–25]. The structure of the weakly bound dripline nucleus  $^{40}\text{Mg}$  is puzzling and intriguing: The lowest  $0^+$  and  $2^+$  states are known and it is not clear how to place a state associated with a second observed  $\gamma$ -ray transition into the spectrum [26]. Recent calculations suggest that the low-lying spectrum signals shape co-existence, and that the coupling to continuum degrees of freedom impacts its structure [27, 28].

In this Letter we revisit even neon and magnesium nuclei from an *ab initio* perspective [29], building on the most recent works [30–32], and aiming at two goals: First, we use the chiral interaction 1.8/2.0 (EM) of Ref. [33] to more accurately predict the structure of the dripline nuclei  $^{34}\text{Ne}$  and  $^{40}\text{Mg}$ ; we also employ an ensemble of chiral potentials to arrive at quantified uncertainties. Second, we employ emulators and a global sensitivity analysis to investigate how chiral interactions impact deformation in this region of the nuclear chart.

The question “What drives nuclear deformation?” has captivated generations of nuclear physicists. We briefly summarize relevant milestones: Bohr [34], Bohr and Mottelson [35], and Nilsson [36] explained deformations as the surface vibrations of a liquid drop and the motion of independent nucleons confined inside [37]. In the 1960s, Baranger and Kumar [38] performed Hartree-Fock Bogoliubov calculations in two active shells and showed that the competition of pairing and quadrupole interactions determine nuclear deformation [39]. A decade later Federman and Pittel [40] demonstrated that deformation in the shell model sets in when isoscalar neutron-proton

interactions dominate over isovector pairing interactions. Dufour and Zuker [41] revisited deformation in the nuclear shell model and found it useful to decompose the Hamiltonian into monopole and multipole parts [42, 43]. Here, the monopole essentially is the one-body normal-ordered term of the shell-model interaction, while the multipole terms are two-body operators; they contain the residual pairing and quadrupole interactions. These results have been succinctly summarized by Zuker’s “Multipole proposes, monopole disposes” [44], i.e., the competition between pairing and quadrupole interactions might suggest deformation while the monopole—the effective spherical mean field—acts as a referee.

We clearly have a good phenomenological understanding about nuclear deformation but lack a more microscopic understanding of which parts of the nucleon-nucleon interaction impact deformation. While the pairing interaction is readily identified with the nucleon-nucleon interaction in the  $^1S_0$  partial wave, the origin of the quadrupole interaction is opaque. With view on Ref. [40], one might be tempted to identify the quadrupole interaction with the isoscalar  $^3D_2$  partial wave (which is attractive). However, the quadrupole interaction is long range—in contrast to the short-range nucleon-nucleon interaction—and it is applicable only in model spaces consisting of one-to-two shells [38]. Thus, our understanding of nuclear deformation is still limited to a low-resolution picture. The *ab initio* computations [30–32, 45–47] reproduced deformed nuclei but did not investigate how they are shaped by the underlying forces. In this work, we seek to understand what impacts deformation at the highest resolution scale possible today, i.e., based on chiral effective field theory (EFT) [48–50]. This is currently as close as we can get in tying low-energy nuclear structure to quantum chromodynamics (QCD) without actually solving QCD.

*Hamiltonian, methods, and model space.*— We use the intrinsic Hamiltonian

$$H = T - T_{\text{CoM}} + V_{NN} + V_{NNN}. \quad (1)$$

Here  $V_{NN}$  is the nucleon-nucleon ( $NN$ ) potential,  $V_{NNN}$  the three-nucleon ( $NNN$ ) potential,  $T$  the total kinetic

energy, and  $T_{\text{CoM}}$  the kinetic energy of the center of mass. We employ the chiral  $NN$  and  $NNN$  interaction 1.8/2.0 (EM) [33], which yields accurate binding energies and spectra of light-, medium-, and heavy-mass nuclei [51–56]. We also used an ensemble of about 100 chiral (next-to-next-to-leading order) NNLO  $NN$  and  $NNN$  interactions with explicit Delta degrees of freedom (with non-local regulators and a momentum cutoff of 394 MeV/ $c$  [57, 58]). This ensemble consists of non-implausible interactions filtered out by history matching [59–61] to scattering phase shifts, deuteron properties, the  $^3\text{H}$ ,  $^4\text{He}$ ,  $^{16}\text{O}$  binding energies and charge radii, and ground- and excited states in  $^{22,24,25}\text{O}$  [62]. We assigned posterior weights conditional on the  $J^\pi = 2^+$  and  $4^+$  rotational states in  $^{24}\text{Ne}$  and then used importance resampling [63, 64] to make posterior predictive distributions for rotational states in other nuclei. Hu *et al.* [61] used a similar approach to predict the neutron-skin thickness of  $^{208}\text{Pb}$ .

Our coupled-cluster computations [65–68] start from an axially symmetric Hartree-Fock reference state with prolate deformation [32, 69]. The inclusion of full  $NNN$  forces increases the computational cost significantly, and we would therefore like to work with the normal-ordered two-body approximation [70–72]. However, the normal-ordered two-body Hamiltonian based on a deformed reference state breaks rotational symmetry. To avoid this problem we follow Frosini *et al.* [73] and first perform a spherical Hartree-Fock computation based on a uniform occupation of the partially filled shells. The resulting density matrix is then used to make the normal-ordered two-body approximation, and the Hamiltonian is finally transformed back to the harmonic oscillator basis. This spherical two-body Hamiltonian is the starting point for our axially symmetric Hartree-Fock computation which yields the reference state  $|\Phi_0\rangle$ .

Our Hartree-Fock computations use a spherical harmonic oscillator basis of up to thirteen major shells while the  $NNN$  interaction is further restricted by an energy cut  $E_{3\text{max}} = 16\hbar\Omega$ . To gauge the convergence of our results we varied the harmonic oscillator frequency ( $\hbar\omega$ ) from 10–16 MeV. Due to computational cost our angular-momentum projected coupled-cluster calculations are restricted to 8–9 major shells, which are sufficient to converge quadrupole deformed states in neon isotopes [32].

We employ the coupled-cluster singles-and-doubles approximation [67]. For a more accurate angular-momentum projection than in Ref. [32] we use the bivariational coupled-cluster energy functional [67, 74, 75]

$$E^{(J)} = \frac{\langle \tilde{\Psi} | P_J H | \Psi \rangle}{\langle \tilde{\Psi} | P_J | \Psi \rangle}. \quad (2)$$

Here  $P_J$  is the angular-momentum projection operator (and contains a rotation operator  $R$ ),  $|\Psi\rangle \equiv e^T |\Phi_0\rangle$  is the right coupled-cluster state and  $\langle \tilde{\Psi} | \equiv \langle \Phi_0 | (1 + \Lambda) e^{-T}$

is the corresponding left ground-state. In the singles-and-doubles approximation of coupled cluster, the excitation operator  $T$  and the de-excitation operator  $\Lambda$  are truncated at the two-particle–two-hole ( $2p$ – $2h$ ) level. We evaluate Eq. (2) via the disentangled approach by Qiu *et al.* [76]. This approach applies the Thouless theorem [77] to act with the rotation operator  $R$  on the symmetry broken reference state, i.e.,  $\langle \Phi_0 | R = \langle \Phi_0 | R | \Phi_0 \rangle \langle \Phi_0 | e^V$ , with  $V$  being a  $1p$ – $1h$  de-excitation operator. Next, one expands  $e^V e^T = e^{W_0 + W_1 + W_2 \dots}$ . The series of  $np$ – $nh$  excitation operators  $W_n$  does not truncate and includes up to  $A$ – $A$  excitations for a nucleus with mass number  $A$ . We only keep the disentangled amplitudes  $W_0, W_1$ , and  $W_2$  and compute them as the solution of a set of ordinary differential equations [76]. The truncation at  $W_2$  implies that the projection operator  $P_J$  is not treated exactly, and angular momentum is only approximately a good quantum number. The Supplemental Material [78] might be useful to experts.

*Results for neon and magnesium isotopes.*— Figures 1 and 2 show the computed energies  $E(2^+)$  and  $E(4^+)$  of the lowest  $2^+$  and  $4^+$  states in the even nuclei  $^{20-32}\text{Ne}$  and  $^{34-40}\text{Mg}$ , respectively, and compares with available data. For neon isotopes, the angular-momentum projected coupled-cluster results based on the 1.8/2.0 (EM) interaction include estimates of uncertainties coming from truncated model-spaces by taking the spread of the results obtained for  $N_{\text{max}} = 6-8$  and  $\hbar\omega = 10-16$  MeV. Using the Delta-full NNLO interaction ensemble we aim to quantify all relevant uncertainties. We employ a fixed model-space of  $N_{\text{max}} = 7$  and  $\hbar\omega = 14$  MeV and assign normally distributed method errors with relative (one sigma) errors of 10% (5%) for  $2^+$  ( $4^+$ ) excitation energies (corresponding to about 100 – 150 keV). Similarly, we assign a 10% relative EFT truncation error for all excitation energies.

Overall, theory agrees with data, though the uncertainties are substantial. For nuclei outside of the island of inversion the ensemble of NNLO Delta-full interactions give somewhat too compressed spectra when comparing centroids to data and to the 1.8/2.0 (EM) interaction (which includes  $NN$  forces at N3LO). Our most precise results are obtained for  $^{32,34}\text{Ne}$ , and the centroids for the ensemble of Delta-full interactions agree with the results for the 1.8/2.0 (EM) interaction. For  $^{34}\text{Ne}$  no data is available, and we predict that the  $2^+$  and  $4^+$  states are similar to the corresponding excited states in  $^{32}\text{Ne}$ . The computed  $R_{42} \equiv E(4^+)/E(2^+)$  values [79] of  $^{34}\text{Ne}$  are  $3.37 \pm 0.13$  for the ensemble (68% confidence interval) and 3.38 for 1.8/2.0 (EM); both are close to the value 10/3 of a rigid rotor. Thus, we expect  $^{34}\text{Ne}$  to be as rotational as  $^{32}\text{Ne}$ . Overall, *ab initio* theory agrees with data, with the exception of  $E(2^+)$  in  $^{30}\text{Ne}$  which is significantly higher than experiment and therefore indicates an artificially large  $N = 20$  shell gap. The persistence of the  $N = 20$  shell gap in this region of the nuclear chart was

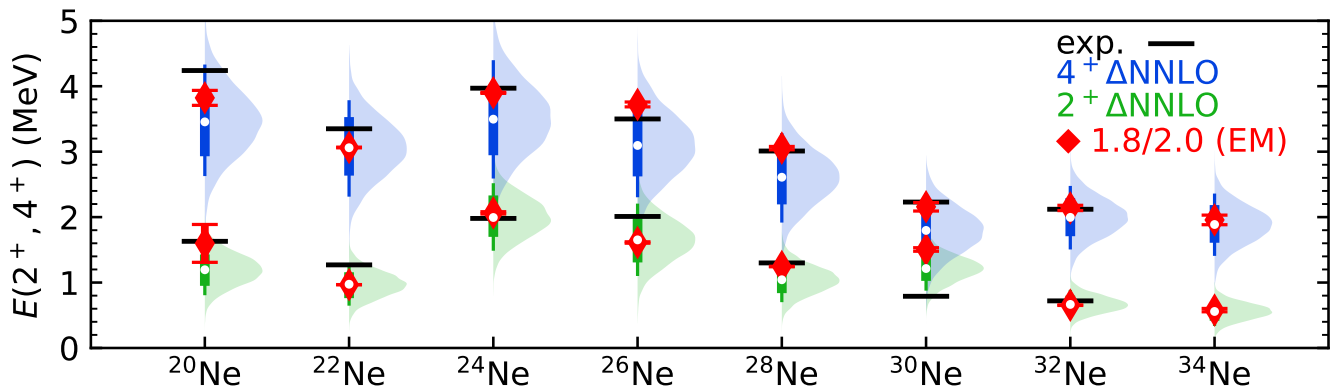


FIG. 1. Energies of lowest  $2^+$  and  $4^+$  states in the even nuclei  $^{20-34}\text{Ne}$ , computed using angular-momentum projected coupled-cluster with the interaction 1.8/2.0 (EM) [33] (red diamonds with uncertainties from finite model-spaces), and posterior predictive distributions from importance resampling using the ensemble of Delta-full ( $\Delta$ ) interactions including sampling of method and model errors (68% and 90% credible intervals as a thick and thin vertical bar, respectively, and the median marked as a white circle) compared to data (black horizontal bars).

also seen in the projected generator-coordinate-method computations of  $^{30}\text{Ne}$  [31] and coupled-cluster computations of charge radii of neutron-rich neon and magnesium isotopes [69]. These findings hint at deficiencies of the employed interactions in correctly describing the boundaries of the island of inversion. One could speculate that our computed  $0^+$  ground-state of  $^{30}\text{Ne}$  corresponds to the observed spherical shape co-existent  $0^+$  state in  $^{32}\text{Mg}$  at 1 MeV of excitation energy [19].

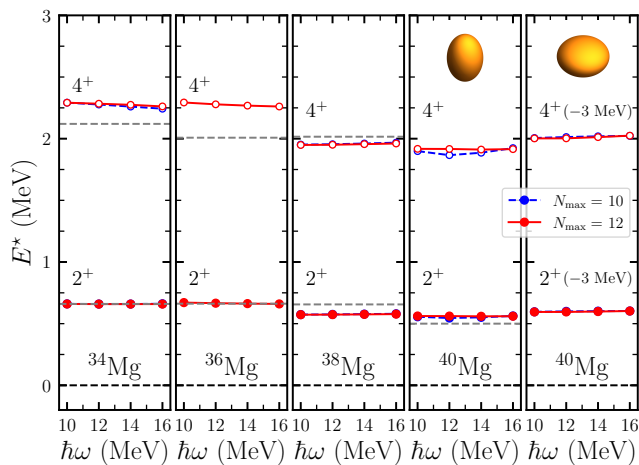


FIG. 2. Energies of lowest  $2^+$  and  $4^+$  states in even nuclei  $^{34-40}\text{Mg}$ , as a function of the oscillator frequency and for various model spaces, computed using projected Hartree-Fock with the chiral interaction 1.8/2.0 (EM) [33] and compared to data (dashed horizontal lines). For  $^{40}\text{Mg}$  we show both the prolate and oblate rotational bands; the latter band head is about 3 MeV above the prolate ground state.

For  $^{34-40}\text{Mg}$  we employ the 1.8/2.0 (EM) interaction and use angular-momentum projected Hartree-Fock in larger model-spaces. This simplification is justified based

on Ref. [32] and the comparison of the rotational bands obtained from Hartree-Fock and coupled-cluster theory in the neon nuclei. For the dripline nucleus  $^{40}\text{Mg}$  we also include coupling to the particle continuum by using a Woods-Saxon basis consisting of bound and scattering states for the neutron  $p_{3/2}$  partial wave, following Ref. [80]. The results are close to data where those are available, see Fig. 2. One expects an inversion of the  $p_{3/2}$  and  $f_{7/2}$  single-particle orbitals close to the magnesium dripline. This is supported by the observation that  $^{37}\text{Mg}$  is a deformed  $p$ -wave halo nucleus [81] and mean-field computations accounting for deformation and continuum coupling [82, 83]. Indeed our calculations for  $^{38,40}\text{Mg}$  show an inversion of the  $\Omega^\pi = 7/2^-$  and  $\Omega^\pi = 1/2^-$  single-particle orbitals (where  $\Omega$  denotes the single-particle angular-momentum component along the axial symmetry axis). We find that  $^{34-40}\text{Mg}$  are all prolate in their ground-state, with rotational bands that are close to data (see Fig. 2). Interestingly, for  $^{40}\text{Mg}$  we also find an oblate Hartree-Fock state that is close in energy to the prolate ground state. Performing coupled-cluster calculations for these two references we find that the oblate band head is about 3 MeV above the prolate ground-state, indicating an onset of shape co-existence and a possible interpretation of the third observed excited state [26]. This picture is also consistent with the Monte-Carlo shell-model computations of Tsunoda *et al.* [27]. Figure 2 shows both the prolate and oblate  $2^+$  and  $4^+$  states, and we observe that the rotational structure of these two bands are very similar and close to that of a rigid rotor.

*Global sensitivity analysis of deformation.*— We want to illuminate how the individual terms of the chiral interaction at NNLO impact deformation in the island-of-inversion nuclei  $^{32,34}\text{Ne}$  and  $^{34}\text{Mg}$ , and compare this to the deformed and stable nucleus  $^{20}\text{Ne}$ . To that

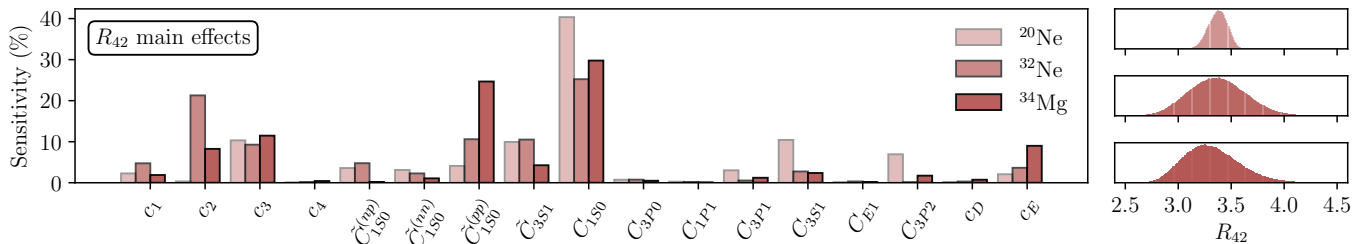


FIG. 3. Main effects of the  $R_{42}$  deformation measure in  $^{20,32}\text{Ne}$  and  $^{34}\text{Mg}$  as obtained in a global sensitivity-analysis of  $10^6$  emulations of projected Hartree-Fock computations using Delta-full chiral EFT at NNLO. Left panel: main effects of the low-energy constants. Right three panels: Histograms of  $R_{42}$  for  $^{20}\text{Ne}$  (top),  $^{32}\text{Ne}$  (middle), and  $^{34}\text{Mg}$  (bottom).

purpose we perform a variance-based global sensitivity-analysis [84, 85] of the ratio  $R_{42}$  in  $^{20,32}\text{Ne}$  and  $^{34}\text{Mg}$ . We partition the total variance of  $R_{42}$  into variances conditional on each of the low-energy constants in chiral EFT. The dimensionless ratio of a conditional variance and the total variance in  $R_{42}$  is called the *main effect*, and a greater value indicates a greater sensitivity of  $R_{42}$  to the corresponding low-energy constant.

We consider all 17 low-energy constants of the Delta-full chiral EFT interaction model in the sensitivity analysis: The leading-order  $S$ -wave contacts  $\tilde{C}_{3S_1}$  and  $\tilde{C}_{1S_0}^{(\tau)}$  with  $\tau = nn, np, pp$  denoting the isospin projections 1, 0,  $-1$ , the subleading contacts  $C_{1S_0}$ ,  $C_{3S_1}$ ,  $C_{3P_0}$ ,  $C_{1P_1}$ ,  $C_{3P_1}$ , and  $C_{3P_2}$  (acting in a partial wave as indicated by the subscript), and  $C_{E_1}$  acting in the the off-diagonal triplet  $S-D$  channel. In addition there are four subleading pion-nucleon couplings  $c_{1,2,3,4}$ , as well as the  $c_D$  and  $c_E$  couplings governing the strengths of the short-range three-nucleon potential.

The variance integrals underlying the sensitivity analysis are evaluated on a hypercubic domain centered on the  $\Delta\text{NNLO}_{\text{GO}}(394)$  parameterization [58]. Drawing on recent Bayesian analyses [86, 87] we use  $\pm 0.05 \text{ GeV}^{-1}$  as the relevant range for each of the pion-nucleon couplings  $c_i$  and  $\pm 0.05 \times 10^2 \text{ GeV}^{-2}$  for the sub-leading constants  $C_i$ . The leading-order contact couplings  $\tilde{C}_i$  are somewhat small (in units of  $10^4 \text{ GeV}^{-4}$ ), in accordance with naturalness expectations, and their intervals are limited to  $\pm 0.005 \times 10^4 \text{ GeV}^{-4}$ . We use Monte Carlo integration to evaluate the variance integrals and this requires  $18 \cdot 2^{16} \approx 10^6$  samples to keep the sampling uncertainty small. Our results are robust when re-scaling all side-lengths of the hypercube by factors of 1/2 and 2. Larger domains result in noticeable higher-order sensitivities which we did not analyze further.

It is sufficiently accurate to solve for the excited-state energies  $E(2^+)$  and  $E(4^+)$  in  $^{20,32}\text{Ne}$  and  $^{34}\text{Mg}$  using projection-after-variation Hartree-Fock [31, 32]. However, the Monte Carlo sampling in a global sensitivity analysis requires prohibitively many projected Hartree-Fock computations. Thus, we develop emulators, i.e., computationally efficient and accurate models that mimic

the full *ab initio* calculation [85, 88], using eigenvector continuation [89] of angular-momentum projected Hartree-Fock. All emulators were trained following a strategy similar to Ref. [85], i.e., using  $N_{\text{train}} = 68$  exact Hartree-Fock states each for the  $0^+$ ,  $2^+$ ,  $4^+$  states and training values for the low-energy constants drawn according to a space-filling latin hypercube design within 20-30% variation of their  $\Delta\text{NNLO}_{\text{GO}}(394)$  values. A comparison with 400 exact Hartree-Fock calculations indicates at most 1% discrepancies (on the  $1\sigma$ -level) for the  $R_{42}$  emulators and even better for the emulation of excitation energies. The Supplemental Material [78] might be useful to experts.

Figure 3 shows the main effects for  $R_{42}$  in  $^{20,32}\text{Ne}$  and  $^{34}\text{Mg}$ . A majority of the output have  $R_{42} \approx 10/3$  which indicates an axially-deformed rigid rotor and emergent symmetry-breaking. We find that more than 97% of the variance in  $R_{42}$  is explained via main effects. For all three nuclei, about 40% of the deformation is driven by the subleading pion-nucleon coupling  $c_3$  and singlet  $S$ -wave contact. The former determines the strength of the NNLO two-pion exchange in the nucleon-nucleon and the three-nucleon potentials. Together with the main effect of  $\tilde{C}$ , proportional to the leading singlet  $S$ -wave contact, we can explain most of the observed variance in  $R_{42}$ . For  $^{34}\text{Mg}$ , with two protons more than  $^{20,32}\text{Ne}$ , deformation becomes more sensitive to the isospin-breaking  $S$ -wave contact in the proton-proton channel. Towards the neutron dripline, deformation is more sensitive to the short-range three-nucleon forces and the pion-nucleon coupling  $c_2$ .

We can also use the ensemble employed in Fig. 1 to probe what impacts deformation. The relevant parts of the nuclear interaction can be identified by studying correlations between the observable  $R_{42}$  in  $^{32}\text{Ne}$  and individual low-energy constants. We find that the correlation is strongest for  $C_{1S_0}$  (with a correlation coefficient  $r = 0.73$ , i.e., an increase in the repulsive  $C_{1S_0}$  increases deformation), but it is also sizeable for the three-nucleon contact  $c_E$ . Comparing these results with the conditional variances from the global sensitivity analysis confirms the importance of pairing via the  $^1S_0$  channel. We note that the domain of low-energy constants used in the global

sensitivity analysis is smaller than the non-implausible volume spanned by the interaction ensemble from history matching.

*Conclusions.*— We reported on *ab initio* computations of neutron-rich neon and magnesium nuclei. For neon, an ensemble of chiral interactions and the 1.8/2.0 (EM) interaction yield accurate results (except for  $N = 20$ ), and we predict that  $^{34}\text{Ne}$  is well deformed. For  $^{34-38}\text{Mg}$  our calculations with the 1.8/2.0 (EM) interaction are close to data, and we predict a prolate ground-state rotational band and an excited oblate band in  $^{40}\text{Mg}$ . A global sensitivity analysis and a study of correlations reveal that a few low-energy constants strongly impact deformation. This is the first step in understanding nuclear deformation at a high resolution scale.

This work was supported by the U.S. Department of Energy, Office of Science, Office of Nuclear Physics, under Award Nos. DE-FG02-96ER40963 and DE-SC0018223, by SciDAC-5 (NUCLEI collaboration), by the Quantum Science Center, a National Quantum Information Science Research Center of the U.S. Department of Energy, by the European Research Council (ERC) under the European Unions Horizon 2020 research and innovation program (Grant Agreement No. 758027), the Swedish Research Council (Grants No. 2017-04234, No. 2020-05127 and No. 2021-04507). Computer time was provided by the Innovative and Novel Computational Impact on Theory and Experiment (INCITE) programme. This research used resources of the Oak Ridge Leadership Computing Facility located at Oak Ridge National Laboratory, which is supported by the Office of Science of the Department of Energy under contract No. DE-AC05-00OR22725 and resources provided by the Swedish National Infrastructure for Computing (SNIC) at Chalmers Centre for Computational Science and Engineering (C3SE), and the National Supercomputer Centre (NSC) partially funded by the Swedish Research Council through grant agreement no. 2018-05973.

- 
- [1] E. K. Warburton, J. A. Becker, and B. A. Brown, “Mass systematics for  $a=29-44$  nuclei: The deformed  $a\sim 32$  region,” *Phys. Rev. C* **41**, 1147–1166 (1990).
- [2] J. Terasaki, H. Flocard, P.-H. Heenen, and P. Bonche, “Deformation of nuclei close to the two-neutron drip line in the mg region,” *Nuclear Physics A* **621**, 706–718 (1997).
- [3] R. R. Rodriguez-Guzman, J. L. Egido, and L. M. Robledo, “Quadrupole collectivity of neutron rich neon isotopes,” *Eur. Phys. J. A* **17**, 37–47 (2003).
- [4] M. Yamagami and Nguyen Van Giai, “Pairing effects on the collectivity of quadrupole states around  $^{32}\text{Mg}$ ,” *Phys. Rev. C* **69**, 034301 (2004).
- [5] Kosho Minomo, Takenori Sumi, Masaaki Kimura, Kazuyuki Ogata, Yoshifumi R. Shimizu, and Masanobu Yahiro, “Deformation effect on total reaction cross sections for neutron-rich ne isotopes,” *Phys. Rev. C* **84**, 034602 (2011).
- [6] Takenori Sumi, Kosho Minomo, Shingo Tagami, Masaaki Kimura, Takuma Matsumoto, Kazuyuki Ogata, Yoshifumi R. Shimizu, and Masanobu Yahiro, “Deformation of ne isotopes in the region of the island of inversion,” *Phys. Rev. C* **85**, 064613 (2012).
- [7] Lulu Li, Jie Meng, P. Ring, En-Guang Zhao, and Shan-Gui Zhou, “Deformed relativistic hartree-bogoliubov theory in continuum,” *Phys. Rev. C* **85**, 024312 (2012).
- [8] E. Caurier, F. Nowacki, and A. Poves, “Merging of the islands of inversion at  $n = 20$  and  $n = 28$ ,” *Phys. Rev. C* **90**, 014302 (2014).
- [9] P. Marević, J.-P. Ebran, E. Khan, T. Nikšić, and D. Vretenar, “Quadrupole and octupole collectivity and cluster structures in neon isotopes,” *Phys. Rev. C* **97**, 024334 (2018).
- [10] S. M. Lukyanov, Yu E. Penionzhkevich, R. Astabatyán, S. Lobastov, Yu Sobolev, D. Guillemaud-Mueller, G. Faivre, F. Ibrahim, A. C. Mueller, F. Pougheon, O. Perru, O. Sorlin, I. Matea, R. Anne, C. Cauvin, R. Hue, G. Georgiev, M. Lewitowicz, F. de Oliveira Santos, D. Verney, Z. Dlouhý, J. Mrázek, D. Baiborodin, F. Negoita, C. Borcea, A. Buta, I. Stefan, and S. Grevy, “Experimental evidence for the particle stability of  $^{34}\text{ne}$  and  $^{37}\text{na}$ ,” *J. Phys. G: Nucl. Part. Phys.* **28**, L41 (2002).
- [11] D. S. Ahn, N. Fukuda, H. Geissel, N. Inabe, N. Iwasa, T. Kubo, K. Kusaka, D. J. Morrissey, D. Murai, T. Nakamura, M. Ohtake, H. Otsu, H. Sato, B. M. Sherrill, Y. Shimizu, H. Suzuki, H. Takeda, O. B. Tarasov, H. Ueno, Y. Yanagisawa, and K. Yoshida, “Location of the neutron dripline at fluorine and neon,” *Phys. Rev. Lett.* **123**, 212501 (2019).
- [12] Y. Yanagisawa, M. Notani, H. Sakurai, M. Kunibu, H. Akiyoshi, N. Aoi, H. Baba, K. Demichi, N. Fukuda, H. Hasegawa, Y. Higurashi, M. Ishihara, N. Iwasa, H. Iwasaki, T. Gomi, S. Kanno, M. Kurokawa, Y. U. Matsuyama, S. Michimasa, T. Minemura, T. Mizoi, T. Nakamura, A. Saito, M. Serata, S. Shimoura, T. Sugimoto, E. Takeshita, S. Takeuchi, K. Ue, K. Yamada, K. Yoneda, and T. Motobayashi, “The first excited state of  $^{30}\text{ne}$  studied by proton inelastic scattering in reversed kinematics,” *Physics Letters B* **566**, 84–89 (2003).
- [13] P. Doornenbal, H. Scheit, N. Aoi, S. Takeuchi, K. Li, E. Takeshita, H. Wang, H. Baba, S. Deguchi, N. Fukuda, H. Geissel, R. Gernhäuser, J. Gibelin, I. Hachiuma, Y. Hara, C. Hinke, N. Inabe, K. Itahashi, S. Itoh, D. Kameda, S. Kanno, Y. Kawada, N. Kobayashi, Y. Kondo, R. Krücken, T. Kubo, T. Kuboki, K. Kusaka, M. Lantz, S. Michimasa, T. Motobayashi, T. Nakamura, T. Nakao, K. Namihira, S. Nishimura, T. Ohnishi, M. Ohtake, N. A. Orr, H. Otsu, K. Ozeki, Y. Satou, S. Shimoura, T. Sumikama, M. Takechi, H. Takeda, K. N. Tanaka, K. Tanaka, Y. Togano, M. Winkler, Y. Yanagisawa, K. Yoneda, A. Yoshida, K. Yoshida, and H. Sakurai, “Spectroscopy of  $^{32}\text{Ne}$  and the “island of inversion”,” *Phys. Rev. Lett.* **103**, 032501 (2009).
- [14] P. Doornenbal, H. Scheit, S. Takeuchi, N. Aoi, K. Li, M. Matsushita, D. Steppenbeck, H. Wang, H. Baba, E. Ideguchi, N. Kobayashi, Y. Kondo, J. Lee, S. Michimasa, T. Motobayashi, A. Poves, H. Sakurai, M. Takechi, Y. Togano, and K. Yoneda, “Mapping the deformation in the “island of inversion”: Inelastic scattering of  $^{30}\text{Ne}$  and  $^{36}\text{Mg}$  at intermediate energies,” *Phys. Rev. C* **93**,

- 044306 (2016).
- [15] I. Murray, M. MacCormick, D. Bazin, P. Doornenbal, N. Aoi, H. Baba, H. Crawford, P. Fallon, K. Li, J. Lee, M. Matsushita, T. Motobayashi, T. Otsuka, H. Sakurai, H. Scheit, D. Steppenbeck, S. Takeuchi, J. A. Tostevin, N. Tsunoda, Y. Utsuno, H. Wang, and K. Yoneda, “Spectroscopy of strongly deformed  $^{32}\text{Ne}$  by proton knockout reactions,” *Phys. Rev. C* **99**, 011302 (2019).
- [16] K. Heyde and J. L. Wood, “Intruder states and shape coexistence in the region  $n$  approximately 20,  $z$  approximately 12,” *Journal of Physics G: Nuclear and Particle Physics* **17**, 135 (1991).
- [17] A. Gade and S. N. Liddick, “Shape coexistence in neutron-rich nuclei,” *Journal of Physics G: Nuclear and Particle Physics* **43**, 024001 (2016).
- [18] Tomoaki Togashi, Yusuke Tsunoda, Takaharu Otsuka, and Noritaka Shimizu, “Quantum phase transition in the shape of  $\text{Zr}$  isotopes,” *Phys. Rev. Lett.* **117**, 172502 (2016).
- [19] K. Wimmer, T. Kröll, R. Krücken, V. Bildstein, R. Gernhäuser, B. Bastin, N. Bree, J. Diriken, P. Van Duppen, M. Huyse, N. Patronis, P. Vermaelen, D. Voulot, J. Van de Walle, F. Wenander, L. M. Fraile, R. Chapman, B. Hadinia, R. Orlandi, J. F. Smith, R. Lutter, P. G. Thirolf, M. Labiche, A. Blazhev, M. Kalkühler, P. Reiter, M. Seidlitz, N. Warr, A. O. Macchiavelli, H. B. Jeppesen, E. Fiori, G. Georgiev, G. Schrieder, S. Das Gupta, G. Lo Bianco, S. Nardelli, J. Butterworth, J. Johansen, and K. Riisager, “Discovery of the shape coexisting  $0^+$  state in  $^{32}\text{Mg}$  by a two neutron transfer reaction,” *Phys. Rev. Lett.* **105**, 252501 (2010).
- [20] T. Motobayashi, Y. Ikeda, K. Ieki, M. Inoue, N. Iwasa, T. Kikuchi, M. Kurokawa, S. Moriya, S. Ogawa, H. Murakami, S. Shimoura, Y. Yanagisawa, T. Nakamura, Y. Watanabe, M. Ishihara, T. Teranishi, H. Okuno, and R. F. Casten, “Large deformation of the very neutron-rich nucleus  $^{32}\text{Mg}$  from intermediate-energy coulomb excitation,” *Phys. Lett. B* **346**, 9 – 14 (1995).
- [21] H. Iwasaki, T. Motobayashi, H. Sakurai, K. Yoneda, T. Gomi, N. Aoi, N. Fukuda, Z. Fülöp, U. Futakami, Z. Gacsi, Y. Higurashi, N. Imai, N. Iwasa, T. Kubo, M. Kunibu, M. Kurokawa, Z. Liu, T. Minemura, A. Saito, M. Serata, S. Shimoura, S. Takeuchi, Y. X. Watanabe, K. Yamada, Y. Yanagisawa, and M. Ishihara, “Large collectivity of  $^{34}\text{Mg}$ ,” *Phys. Lett. B* **522**, 227–232 (2001).
- [22] J. A. Church, C. M. Campbell, D.-C. Dinca, J. Enders, A. Gade, T. Glasmacher, Z. Hu, R. V. F. Janssens, W. F. Mueller, H. Olliver, B. C. Perry, L. A. Riley, and K. L. Yurkewicz, “Measurement of  $e2$  transition strengths in  $^{32,34}\text{Mg}$ ,” *Phys. Rev. C* **72**, 054320 (2005).
- [23] Z. Elekes, Zs. Dombrádi, A. Saito, N. Aoi, H. Baba, K. Demichi, Zs. Fülöp, J. Gibelin, T. Gomi, H. Hasegawa, N. Imai, M. Ishihara, H. Iwasaki, S. Kanno, S. Kawai, T. Kishida, T. Kubo, K. Kurita, Y. Matsuyama, S. Michimasa, T. Minemura, T. Motobayashi, M. Notani, T. Ohnishi, H. J. Ong, S. Ota, A. Ozawa, H. K. Sakai, H. Sakurai, S. Shimoura, E. Takeshita, S. Takeuchi, M. Tamaki, Y. Togano, K. Yamada, Y. Yanagisawa, and K. Yoneda, “Proton inelastic scattering studies at the borders of the “island of inversion”: The  $^{30,31}\text{Na}$  and  $^{33,34}\text{Mg}$  case,” *Phys. Rev. C* **73**, 044314 (2006).
- [24] T. Baumann, A. M. Amthor, D. Bazin, B. A. Brown, C. M. Folden, A. Gade, T. N. Ginter, M. Hausmann, M. Matos, D. J. Morrissey, M. Portillo, A. Schiller, B. M. Sherrill, A. Stolz, O. B. Tarasov, and M. Thoennessen, “Discovery of  $40\text{mg}$  and  $42\text{al}$  suggests neutron drip-line slant towards heavier isotopes,” *Nature* **449**, 1022 – 1024 (2007).
- [25] S. Michimasa, Y. Yanagisawa, K. Inafuku, N. Aoi, Z. Elekes, Zs. Fülöp, Y. Ichikawa, N. Iwasa, K. Kurita, M. Kurokawa, T. Machida, T. Motobayashi, T. Nakamura, T. Nakabayashi, M. Notani, H. J. Ong, T. K. Onishi, H. Otsu, H. Sakurai, M. Shinohara, T. Sumikama, S. Takeuchi, K. Tanaka, Y. Togano, K. Yamada, M. Yamaguchi, and K. Yoneda, “Quadrupole collectivity in island-of-inversion nuclei  $^{28,30}\text{Ne}$  and  $^{34,36}\text{Mg}$ ,” *Phys. Rev. C* **89**, 054307 (2014).
- [26] H. L. Crawford, P. Fallon, A. O. Macchiavelli, P. Doornenbal, N. Aoi, F. Browne, C. M. Campbell, S. Chen, R. M. Clark, M. L. Cortés, M. Cromaz, E. Ideguchi, M. D. Jones, R. Kanungo, M. MacCormick, S. Momiyama, I. Murray, M. Niikura, S. Paschalis, M. Petri, H. Sakurai, M. Salathe, P. Schrock, D. Steppenbeck, S. Takeuchi, Y. K. Tanaka, R. Taniuchi, H. Wang, and K. Wimmer, “First spectroscopy of the near drip-line nucleus  $^{40}\text{Mg}$ ,” *Phys. Rev. Lett.* **122**, 052501 (2019).
- [27] Naofumi Tsunoda, Takaharu Otsuka, Kazuo Takayanagi, Noritaka Shimizu, Toshio Suzuki, Yutaka Utsuno, Sota Yoshida, and Hideki Ueno, “The impact of nuclear shape on the emergence of the neutron dripline,” *Nature* **587**, 66–71 (2020).
- [28] A. O. Macchiavelli, H. L. Crawford, P. Fallon, R. M. Clark, and A. Poves, “Weak binding effects on the structure of  $^{40}\text{Mg}$ ,” *The European Physical Journal A* **58**, 66 (2022).
- [29] A. Ekström, C. Forssén, G. Hagen, G. R. Jansen, W. Jiang, and T. Papenbrock, “What is ab initio in nuclear theory?” *Front. Phys.* **11**, 1129094 (2023), arXiv:2212.11064 [nucl-th].
- [30] T. Miyagi, S. R. Stroberg, J. D. Holt, and N. Shimizu, “Ab initio multishell valence-space hamiltonians and the island of inversion,” *Phys. Rev. C* **102**, 034320 (2020).
- [31] Mikael Frosini, Thomas Duguet, Jean-Paul Ebran, Benjamin Bally, Tobias Mongelli, Tomás R. Rodríguez, Robert Roth, and Vittorio Somà, “Multi-reference many-body perturbation theory for nuclei: II. Ab initio study of neon isotopes via PGCM and IM-NCSM calculations,” *Eur. Phys. J. A* **58**, 63 (2022), arXiv:2111.00797 [nucl-th].
- [32] G. Hagen, S. J. Novario, Z. H. Sun, T. Papenbrock, G. R. Jansen, J. G. Lietz, T. Duguet, and A. Tichai, “Angular-momentum projection in coupled-cluster theory: Structure of  $^{34}\text{Mg}$ ,” *Phys. Rev. C* **105**, 064311 (2022).
- [33] K. Hebeler, S. K. Bogner, R. J. Furnstahl, A. Nogga, and A. Schwenk, “Improved nuclear matter calculations from chiral low-momentum interactions,” *Phys. Rev. C* **83**, 031301 (2011).
- [34] Aage Bohr, “The coupling of nuclear surface oscillations to the motion of individual nucleons,” *Dan. Mat. Fys. Medd.* **26**, no. 14 (1952).
- [35] Aage Bohr and Ben R. Mottelson, “Collective and individual-particle aspects of nuclear structure,” *Dan. Mat. Fys. Medd.* **27**, no. 16 (1953).
- [36] S. G. Nilsson, “Binding states of individual nucleons in strongly deformed nuclei,” *K. Dan. Vidensk. Selsk. Mat.*

- Fys. Medd. **29**, no.16 (1955).
- [37] A. Bohr and B. R. Mottelson, *Nuclear Structure*, Vol. II: Nuclear Deformation (W. A. Benjamin, Reading, Massachusetts, USA, 1975).
- [38] Michel Baranger and Krishna Kumar, “Nuclear deformations in the pairing-plus-quadrupole model: (ii). discussion of validity of the model,” *Nuclear Physics A* **110**, 490–528 (1968).
- [39] Krishna Kumar and Michel Baranger, “Nuclear deformations in the pairing-plus-quadrupole model: (iii). static nuclear shapes in the rare-earth region,” *Nuclear Physics A* **110**, 529–554 (1968).
- [40] P. Federman and S. Pittel, “Unified shell-model description of nuclear deformation,” *Phys. Rev. C* **20**, 820–829 (1979).
- [41] Marianne Dufour and Andrés P. Zuker, “Realistic collective nuclear hamiltonian,” *Phys. Rev. C* **54**, 1641–1660 (1996).
- [42] Andrés P. Zuker and Marianne Dufour, “Separation of the monopole contribution to the nuclear Hamiltonian,” arXiv e-prints , nucl-th/9505012 (1995), arXiv:nucl-th/9505012 [nucl-th].
- [43] J. Dufflo and A. P. Zuker, “The nuclear monopole hamiltonian,” *Phys. Rev. C* **59**, R2347–R2350 (1999).
- [44] Alfredo Poves, “Shape coexistence and islands of inversion monopole vs multipole,” *JPS Conference Proceedings* **23**, 012015 (2018).
- [45] M. A. Caprio, P. Maris, J. P. Vary, and R. Smith, “Collective rotation from ab initio theory,” *Int. J. Mod. Phys. E* **24**, 1541002 (2015).
- [46] T. Dytrych, K. D. Launey, J. P. Draayer, D. J. Rowe, J. L. Wood, G. Rosensteel, C. Bahri, D. Langr, and R. B. Baker, “Physics of nuclei: Key role of an emergent symmetry,” *Phys. Rev. Lett.* **124**, 042501 (2020).
- [47] K. S. Becker, K. D. Launey, A. Ekström, and T. Dytrych, “Ab initio symmetry-adapted emulator for studying emergent collectivity and clustering in nuclei,” *Frontiers in Physics* **11** (2023), 10.3389/fphy.2023.1064601.
- [48] E. Epelbaum, H. Krebs, and U.-G. Meißner, “ $\Delta$ -excitations and the three-nucleon force,” *Nucl. Phys. A* **806**, 65 – 78 (2008).
- [49] R. Machleidt and D.R. Entem, “Chiral effective field theory and nuclear forces,” *Phys. Rep.* **503**, 1 – 75 (2011).
- [50] H. W. Hammer, S. König, and U. van Kolck, “Nuclear effective field theory: status and perspectives,” *Rev. Mod. Phys.* **92**, 025004 (2020), arXiv:1906.12122 [nucl-th].
- [51] G. Hagen, A. Ekström, C. Forssén, G. R. Jansen, W. Nazarewicz, T. Papenbrock, K. A. Wendt, S. Bacca, N. Barnea, B. Carlsson, C. Drischler, K. Hebeler, M. Hjorth-Jensen, M. Miorelli, G. Orlandini, A. Schwenk, and J. Simonis, “Neutron and weak-charge distributions of the  $^{48}\text{Ca}$  nucleus,” *Nature Physics* **12**, 186 (2016).
- [52] G. Hagen, G. R. Jansen, and T. Papenbrock, “Structure of  $^{78}\text{Ni}$  from first-principles computations,” *Phys. Rev. Lett.* **117**, 172501 (2016).
- [53] J. Simonis, S. R. Stroberg, K. Hebeler, J. D. Holt, and A. Schwenk, “Saturation with chiral interactions and consequences for finite nuclei,” *Phys. Rev. C* **96**, 014303 (2017).
- [54] T. D. Morris, J. Simonis, S. R. Stroberg, C. Stumpf, G. Hagen, J. D. Holt, G. R. Jansen, T. Papenbrock, R. Roth, and A. Schwenk, “Structure of the lightest tin isotopes,” *Phys. Rev. Lett.* **120**, 152503 (2018).
- [55] P. Gysbers, G. Hagen, J. D. Holt, G. R. Jansen, T. D. Morris, P. Navrátil, T. Papenbrock, S. Quaglioni, A. Schwenk, S. R. Stroberg, and K. A. Wendt, “Discrepancy between experimental and theoretical  $\beta$ -decay rates resolved from first principles,” *Nature Physics* **15**, 428–431 (2019).
- [56] K. Hebeler, V. Durant, J. Hoppe, M. Heinz, A. Schwenk, J. Simonis, and A. Tichai, “Normal ordering of three-nucleon interactions for ab initio calculations of heavy nuclei,” *Phys. Rev. C* **107**, 024310 (2023).
- [57] A. Ekström, G. Hagen, T. D. Morris, T. Papenbrock, and P. D. Schwartz, “ $\Delta$  isobars and nuclear saturation,” *Phys. Rev. C* **97**, 024332 (2018).
- [58] W. G. Jiang, A. Ekström, C. Forssén, G. Hagen, G. R. Jansen, and T. Papenbrock, “Accurate bulk properties of nuclei from  $A = 2$  to  $\infty$  from potentials with  $\Delta$  isobars,” arXiv e-prints , arXiv:2006.16774 (2020), arXiv:2006.16774 [nucl-th].
- [59] Ian Vernon, Michael Goldstein, and Richard G. Bower, “Galaxy formation: a bayesian uncertainty analysis,” *Bayesian Anal.* **5**, 619–669 (2010).
- [60] Ian Vernon, Junli Liu, Michael Goldstein, James Rowe, Jen Topping, and Keith Lindsey, “Bayesian uncertainty analysis for complex systems biology models: emulation, global parameter searches and evaluation of gene functions,” *BMC Systems Biology* **12**, 1 (2018).
- [61] Baishan Hu, Weiguang Jiang, Takayuki Miyagi, Zhonghao Sun, Andreas Ekström, Christian Forssén, Gaute Hagen, Jason D. Holt, Thomas Papenbrock, S. Ragnar Stroberg, and Ian Vernon, “Ab initio predictions link the neutron skin of 208pb to nuclear forces,” *Nature Physics* **18**, 1196–1200 (2022).
- [62] Y. Kondo *et al.*, (2023), in preparation.
- [63] A. F. M. Smith and A. E. Gelfand, “Bayesian statistics without tears: A sampling-resampling perspective,” *Am. Stat.* **46**, 84–88 (1992).
- [64] Weiguang Jiang and Christian Forssén, “Bayesian probability updates using sampling/importance resampling: Applications in nuclear theory,” *Front. in Phys.* **10**, 1058809 (2022), arXiv:2210.02507 [nucl-th].
- [65] H. Kümmel, K. H. Lührmann, and J. G. Zabolitzky, “Many-fermion theory in expS- (or coupled cluster) form,” *Phys. Rep.* **36**, 1 – 63 (1978).
- [66] R. F. Bishop, “An overview of coupled cluster theory and its applications in physics,” *Theoretical Chemistry Accounts: Theory, Computation, and Modeling (Theoretica Chimica Acta)* **80**, 95–148 (1991).
- [67] Rodney J. Bartlett and Monika Musiał, “Coupled-cluster theory in quantum chemistry,” *Rev. Mod. Phys.* **79**, 291–352 (2007).
- [68] G. Hagen, T. Papenbrock, M. Hjorth-Jensen, and D. J. Dean, “Coupled-cluster computations of atomic nuclei,” *Rep. Prog. Phys.* **77**, 096302 (2014).
- [69] S. J. Novario, G. Hagen, G. R. Jansen, and T. Papenbrock, “Charge radii of exotic neon and magnesium isotopes,” *Phys. Rev. C* **102**, 051303 (2020).
- [70] G. Hagen, T. Papenbrock, D. J. Dean, A. Schwenk, A. Nogga, M. Włoch, and P. Piecuch, “Coupled-cluster theory for three-body Hamiltonians,” *Phys. Rev. C* **76**, 034302 (2007).
- [71] Robert Roth, Sven Binder, Klaus Vobig, Angelo Calci, Joachim Langhammer, and Petr Navrátil, “Medium-Mass Nuclei with Normal-Ordered Chiral  $NN+3N$  In-

- teractions,” *Phys. Rev. Lett.* **109**, 052501 (2012).
- [72] Sven Binder, Piotr Piecuch, Angelo Calci, Joachim Langhammer, Petr Navrátil, and Robert Roth, “Extension of coupled-cluster theory with a noniterative treatment of connected triply excited clusters to three-body hamiltonians,” *Phys. Rev. C* **88**, 054319 (2013).
- [73] M. Frosini, T. Duguet, B. Bally, Y. Beaujeault-Taudière, J. P. Ebran, and V. Somà, “In-medium  $k$ -body reduction of  $n$ -body operators: A flexible symmetry-conserving approach based on the sole one-body density matrix,” *Eur. Phys. J. A* **57**, 151 (2021).
- [74] J. Arponen, “The method of stationary cluster amplitudes and the phase transition in the lipkin pseudospin model,” *Journal of Physics G: Nuclear Physics* **8**, L129 (1982).
- [75] Jouko Arponen, “Variational principles and linked-cluster expansion for static and dynamic many-body problems,” *Ann. Phys.* **151**, 311 – 382 (1983).
- [76] Yiheng Qiu, Thomas M. Henderson, Jinmo Zhao, and Gustavo E. Scuseria, “Projected coupled cluster theory,” *J. Chem. Phys.* **147**, 064111 (2017).
- [77] D. J. Thouless, “Stability conditions and nuclear rotations in the Hartree-Fock theory,” *Nuclear Physics* **21**, 225–232 (1960).
- [78] Z. H. Sun, A. Ekström, C. Forssén, G. Hagen, and T. Papenbrock, “Supplemental material to this work,” (2023).
- [79] R. F. Casten, *Nuclear Structure from a Simple Perspective*, Oxford Studies in Nuclear Physics, Vol. 13 (Oxford University Press, New York, 1990).
- [80] G. Hagen, M. Hjorth-Jensen, G. R. Jansen, and T. Papenbrock, “Emergent properties of nuclei from ab initio coupled-cluster calculations,” *Phys. Scr.* **91**, 063006 (2016).
- [81] N. Kobayashi, T. Nakamura, Y. Kondo, J. A. Tostevin, Y. Utsuno, N. Aoi, H. Baba, R. Barthelemy, M. A. Famiانو, N. Fukuda, N. Inabe, M. Ishihara, R. Kanungo, S. Kim, T. Kubo, G. S. Lee, H. S. Lee, M. Matsushita, T. Motobayashi, T. Ohnishi, N. A. Orr, H. Otsu, T. Otsuka, T. Sako, H. Sakurai, Y. Satou, T. Sumikama, H. Takeda, S. Takeuchi, R. Tanaka, Y. Togano, and K. Yoneda, “Observation of a  $p$ -wave one-neutron halo configuration in  $^{37}\text{Mg}$ ,” *Phys. Rev. Lett.* **112**, 242501 (2014).
- [82] Ikuko Hamamoto, “Neutron shell structure and deformation in neutron-drip-line nuclei,” *Phys. Rev. C* **85**, 064329 (2012).
- [83] Ikuko Hamamoto, “Shell structure of one-particle resonances in deformed potentials,” *Phys. Rev. C* **93**, 054328 (2016).
- [84] I. M. Sobol, “Global sensitivity indices for nonlinear mathematical models and their Monte Carlo estimates,” *Math. Comput. Simul.* **55**, 271–280 (2001).
- [85] Andreas Ekström and Gaute Hagen, “Global sensitivity analysis of bulk properties of an atomic nucleus,” *Phys. Rev. Lett.* **123**, 252501 (2019).
- [86] S. Wesolowski, I. Svensson, A. Ekström, C. Forssén, R. J. Furnstahl, J. A. Melendez, and D. R. Phillips, “Rigorous constraints on three-nucleon forces in chiral effective field theory from fast and accurate calculations of few-body observables,” *Phys. Rev. C* **104**, 064001 (2021), arXiv:2104.04441 [nucl-th].
- [87] Isak Svensson, Andreas Ekström, and Christian Forssén, “Inference of the low-energy constants in delta-full chiral effective field theory including a correlated truncation error,” arXiv (2023), arXiv:2304.02004 [nucl-th].
- [88] S. König, A. Ekström, K. Hebeler, D. Lee, and A. Schwenk, “Eigenvector Continuation as an Efficient and Accurate Emulator for Uncertainty Quantification,” *Phys. Lett. B* **810**, 135814 (2020), arXiv:1909.08446 [nucl-th].
- [89] Dillon Frame, Rongzheng He, Ilse Ipsen, Daniel Lee, Dean Lee, and Ermal Rrapaj, “Eigenvector continuation with subspace learning,” *Phys. Rev. Lett.* **121**, 032501 (2018)

**SUPPLEMENTAL MATERIAL: HOW CHIRAL  
FORCES SHAPE NEUTRON-RICH NE AND MG  
NUCLEI**

**Convergence of projection-after-variation  
Hartree-Fock and the disentangled coupled-cluster  
approach**

Figure 4 shows the  $2^+$  and  $4^+$  rotational states in  $^{20}\text{Ne}$  obtained with the  $\text{NNLO}_{\text{opt}}$  nucleon-nucleon interaction [91], and using the projection-after-variation Hartree-Fock and disentangled approaches with the “naive” and the bi-variational (linear-response) coupled-cluster ansatz [76], respectively. We observe that both states are well converged with respect to the model-space size for projection-after-variation Hartree-Fock. For the disentangled approach there is a slightly larger dependence on the employed model-space. This is likely so because the disentangled coupled-cluster approach does not restore the broken symmetry exactly [32, 76]. We also observe that projection-after-variation Hartree-Fock and the bi-variational disentangled coupled-cluster agree with benchmarks from symmetry-adapted no-core shell-model calculations [93], while the “naive” disentangled approach yields more compressed spectra.

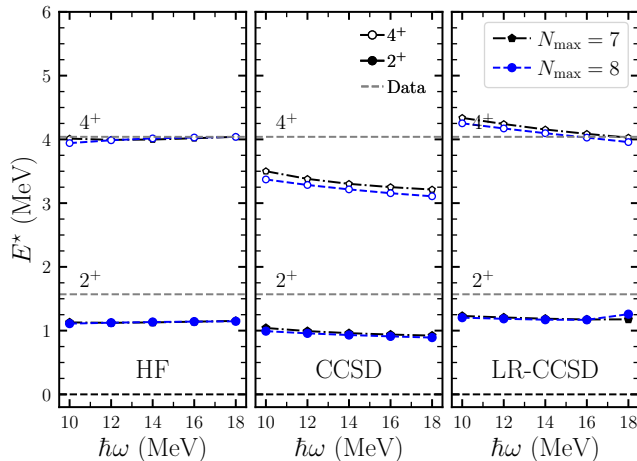


FIG. 4. Comparison between projection-after-variation Hartree Fock (HF), projected coupled-cluster (CCSD), and projected linear-response coupled-cluster method (LR-CCSD) for the excited  $2^+$  and  $4^+$  in  $^{20}\text{Ne}$  using the  $\text{NNLO}_{\text{opt}}$  nucleon-nucleon interaction. The dashed lines show the results from symmetry-adapted no-core shell-model computations using the same interaction.

Figure 5 shows the  $2^+$  and  $4^+$  excited states in  $^{20-34}\text{Ne}$  obtained with the interaction 1.8/2.0 (EM) [33] and compared to data for different model-space sizes. We find (with the exception of  $^{20}\text{Ne}$  at  $\hbar\omega = 16$  MeV) that the states are well converged with respect to model-space size. The variation of the results with respect to the model-space is shown as an uncertainty in Fig. 1 in the

main text.

**Emulating projection-after-variation Hartree-Fock  
using eigenvector continuation**

To construct the Hartree-Fock emulators we exploit that the Delta-full NNLO Hamiltonian can be written in a form that depends linearly on the 17 low-energy constants ( $\vec{\alpha}$ ) of interest, i.e.,

$$H(\vec{\alpha}) = H_0 + \sum_{i=1}^{17} \alpha_i H_i. \quad (3)$$

Here,  $H_0 = T_{\text{kin}} + V_0$  is independent of the low-energy constants we consider here and includes the intrinsic kinetic energy  $T_{\text{kin}}$  and potential terms  $V_0$  such as one-pion exchange, leading two-pion exchange, and the Fujita-Miyazawa [92] three-nucleon interaction.

To proceed we write the full Hamiltonian in normal-ordered form with respect to an arbitrary Hartree-Fock reference state, i.e.  $H = E_{\text{HF}} + F + W$ . Here  $E_{\text{HF}}$  corresponds to the Hartree-Fock (vacuum) energy,  $F$  is the Fock-matrix (i.e. the normal-ordered one-body term), and  $W$  contains two- and three-body normal-ordered terms. We note that  $F$  is diagonal in the Hartree-Fock representation. We can then write the one-body Hartree-Fock Hamiltonian as  $H_{\text{HF}} = E_{\text{HF}} + F$ . We seek to emulate the Hartree-Fock energy for some target value  $\vec{\alpha} = \vec{\alpha}_{\odot}$ . To that end, we expand the target wave-function in a set of Hartree-Fock states  $|\phi_{\odot}\rangle = \sum_i^{n_i} c_i |\phi_i\rangle$ , where  $|\phi_i\rangle$  is a Hartree-Fock state obtained for the training point of low-energy constants  $\vec{\alpha}_i$ , i.e.

$$H_{\text{HF}}(\vec{\alpha}_i)|\phi_i\rangle = E_{\text{HF}}(\vec{\alpha}_i)|\phi_i\rangle, \quad (4)$$

and  $H_{\text{HF}}(\vec{\alpha}_i)$  is the Hartree-Fock Hamiltonian for  $\vec{\alpha}_i$ . The emulator step relies on expressing the eigenstates of the target Hamiltonian  $H_{\text{HF}}(\vec{\alpha}_{\odot})$  as the solution to the generalized eigenvalue problem

$$\sum_{ij} \langle \phi_i | H_{\text{HF}}(\vec{\alpha}_{\odot}) | \phi_j \rangle c_j = E_{\odot} \sum_{ij} \langle \phi_i | \phi_j \rangle c_j, \quad (5)$$

where  $E_{\odot} \approx E_{\text{HF}}(\vec{\alpha}_{\odot})$  and the sums run over the  $N_{\text{train}}$  eigenstates obtained during the training step. In the following we write  $h = H_{\text{HF}}$  for simplicity of notation. To evaluate the norm and Hamiltonian kernels we utilize the Thouless theorem [77], and follow an approach similar to the one used for the disentangled coupled-cluster approach [76].

The Hartree-Fock solution  $|\phi_i\rangle$  for training point  $\vec{\alpha}_i$  is connected to the Harmonic oscillator unrestricted reference state  $|\Phi_0\rangle$  via a unitary transformation, i.e.  $|\phi_i\rangle = U_i|\Phi_0\rangle$ . The norm and Hamiltonian kernels for eigenvector continuation are

$$\langle \phi_i | \phi_j \rangle = \langle \Phi_0 | \mathcal{O}_{ij} | \Phi_0 \rangle, \quad (6)$$

$$\langle \phi_i | h(\vec{\alpha}_{\odot}) | \phi_j \rangle = \langle \Phi_0 | \mathcal{O}_{ij} h_j(\vec{\alpha}_{\odot}) | \Phi_0 \rangle. \quad (7)$$

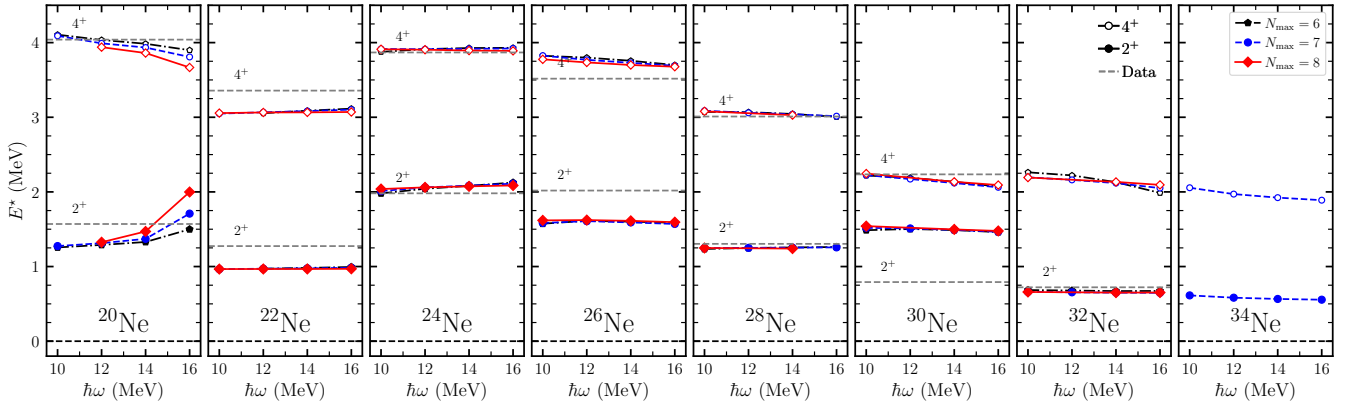


FIG. 5. Energies  $E$  of the lowest  $2^+$  and  $4^+$  states in even nuclei  $^{20-34}\text{Ne}$ , computed with the interaction 1.8/2.0 (EM) from chiral effective field theory [33] and compared to data.

Here  $\mathcal{O}_{ij} = U_i^\dagger U_j$  is a unitary matrix, and  $h_j(\vec{\alpha}_\otimes)$  is the target Hamiltonian normal-ordered with respect to the Hartree-Fock state of training point  $\vec{\alpha}_j$ , i.e.  $h_j(\vec{\alpha}_\otimes) = u_j^\dagger h(\vec{\alpha}_\otimes) u_j$ . We note that the Hamiltonian kernel in Eq. (7) is not symmetric, and the Fock matrix,  $F_j(\vec{\alpha}_\otimes)$ , is not diagonal for  $\vec{\alpha}_\otimes \neq \vec{\alpha}_j$ . This is an important point and it ensures that – at a training point – the solution of the generalized eigenvalue problem is indeed an eigenstate of the Hartree-Fock Hamiltonian (and not a generator-coordinate-method solution that is lower in energy). The norm kernel for non-orthogonal reference states is given by [95]

$$\langle \Phi_0 | \mathcal{O}_{ij} | \Phi_0 \rangle = \det(\mathcal{O}_{ij}^{hh}), \quad (8)$$

here  $\mathcal{O}_{ij}^{hh}$  is the matrix of overlaps between occupied (hole) states in  $\langle \phi_i |$  and  $|\phi_j \rangle$ . To evaluate the Hamiltonian kernel we utilize the Thouless theorem [77] and write,

$$\langle \Phi_0 | \mathcal{O}_{ij} = \langle \Phi_0 | \mathcal{O}_{ij} | \Phi_0 \rangle \langle \Phi_0 | e^V, \quad (9)$$

with  $V$  being a  $1p-1h$  de-excitation operator. The matrix elements of  $V$  in the hole-particle ( $hp$ ) space is given by the matrix product [76],

$$V^{hp} = (\mathcal{O}_{ij}^{hh})^{-1} \mathcal{O}_{ij}^{hp}. \quad (10)$$

Inserting Eq. (9) into Eq. (7) we obtain the algebraic equation,

$$\langle \phi_i | H_{\text{HF}}(\vec{\alpha}_\otimes) | \phi_j \rangle = \langle \phi_i | \phi_j \rangle \left( E_{\text{HF}} + \sum_{hp} V_p^h F_h^p \right). \quad (11)$$

Here  $E_{\text{HF}}$  and  $F$  are the vacuum energy and one-body normal ordered terms, respectively, of  $H_{\text{HF}}(\vec{\alpha}_\otimes)$  with respect to  $|\phi_j \rangle$ .

We note that the norm and Hamiltonian Hartree-Fock kernels can also be evaluated using a generalized

Wick's theorem [90, 94–96]. We verified that this alternative approach gives results that agree with the one used in this work. Having obtained the emulated target Hartree-Fock state by diagonalizing the generalized non-symmetric eigenvalue problem in Eq. (5), we evaluate the projected target Hartree-Fock energies from

$$E_\otimes^{(J)} = \frac{\langle \phi_\otimes | P_J H(\vec{\alpha}_\otimes) | \phi_\otimes \rangle}{\langle \phi_\otimes | P_J | \phi_\otimes \rangle}. \quad (12)$$

Here the full target Hamiltonian in Eq. (3) enters, and  $P_J$  is the projection operator.

### Sensitivity analysis of deformation in neutron-rich neon isotopes

Figure 6 shows the main effects for the  $R_{42}$  ratios and the ground and excited state energies (i.e.,  $E(0^+)$ ,  $E(2^+)$ , and  $E(4^+)$ ) in  $^{20,32}\text{Ne}$  and  $^{34}\text{Mg}$ . All results are based on the same set of samples as in the main text. Here, we also include the total effects [97] (shown as white bars on top of colored bars of the main effects) and they are nearly identical to the main effects. This indicates that the (sum of) higher-order sensitivities are very small in the present domain.

The main effects for the  $R_{42}$  ratios is discussed in the main text. Here we comment of the energies  $E(0^+)$ ,  $E(2^+)$ , and  $E(4^+)$ . There are three main trends in Fig. 6. First, the variance of  $E(0^+)$ , i.e., the energy of the ground state, is explained almost entirely by the subleading pion-nucleon coupling  $c_2$  and the leading  $S$ -wave contact  $\tilde{C}_{3S_1}$  in all three nuclei. The latter coupling is directly proportional to the deuteron binding energy. Second, the main effects are distributed over more couplings for the nuclei  $^{32}\text{Ne}$  and  $^{34}\text{Mg}$  that are closer to the neutron dripline. Third, the ground and excited state energies exhibit different main effect patterns for neutron-rich Ne and Mg compared to  $^{20}\text{Ne}$  indicating that the structure of their

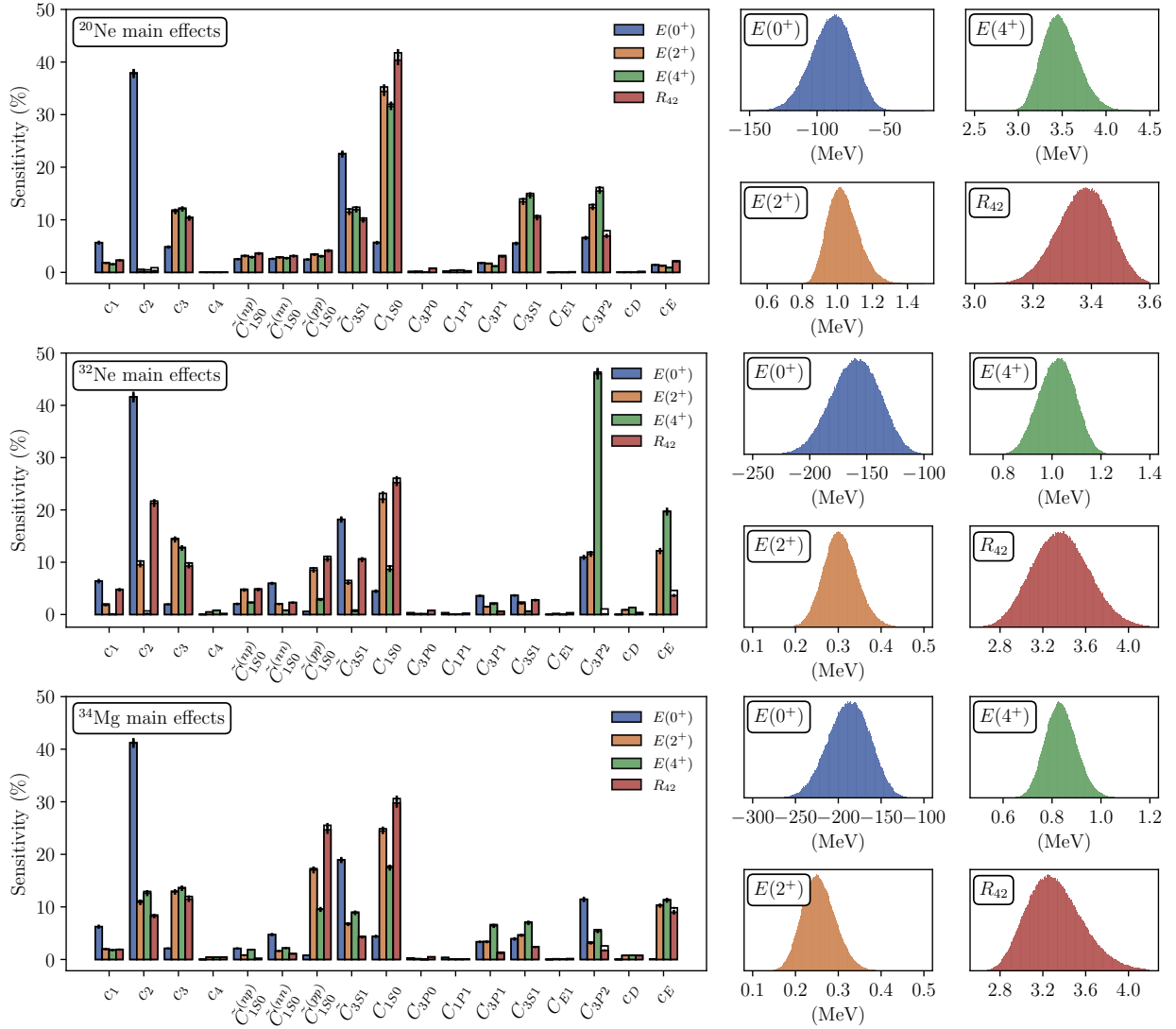


FIG. 6. Results of the global sensitivity-analysis for the structure of  $^{20,32}\text{Ne}$  and  $^{34}\text{Mg}$  (top, center, and bottom panels). All Monte Carlo samples obtained as in the main text. Left panels: the main effects (colored bars) for  $R_{42}$  ground state energy ( $E_{gs}$ ) and excited  $2^+$  and  $4^+$  states. The vertical black bars indicate the respective 95% confidence intervals of the sensitivity indices as obtained using bootstrapped sampling. Here we also include total effects (white bars on top). Groups of right four panels: histograms displaying the variation of the 1,179,648 samples for each output. All energies were obtained using an emulator based on eigenvector continuation of projected Hartree-Fock.

respective wave functions likely differ.

Figure 7 shows the accuracy of the  $R_{42}$  emulators as measured by comparison with exact projected Hartree-Fock calculations. The standard deviation of the differences indicates a relative precision of 1% for the interval of  $R_{42}$  values relevant to the global sensitivity analysis. The emulation of excitation energies is accurate on the 10 keV level.

### Correlation analysis of deformation in neutron-rich neon isotopes

Figure 8 shows the strongest correlations between the low-energy constants of the Delta-full NNLO Hamiltonian and the observables  $R_{42}$  and  $E(2^+)$  of  $^{32}\text{Ne}$  for the ensemble of interactions from history matching.

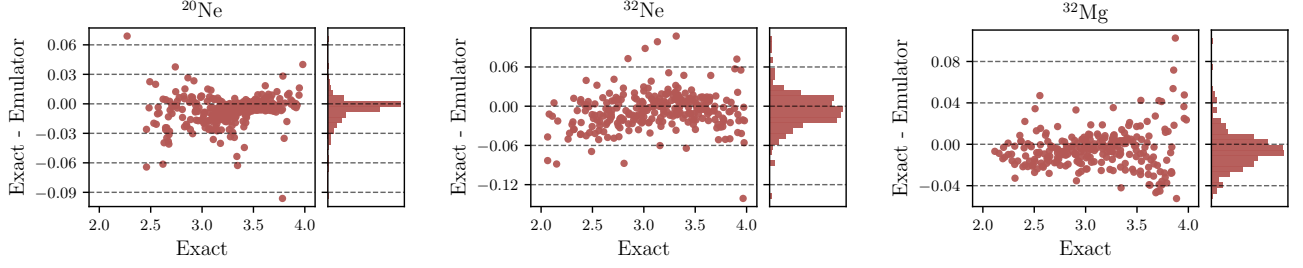


FIG. 7. Accuracy of the  $R_{42}$  emulator as measured by the difference with respect to 400 exact calculations. Shown are the subsets of results for which  $R_{42} \in [2, 4]$ , i.e., the range relevant to the global sensitivity analysis. The horizontal dashed lines indicate precision as they are spaced by two standard deviations of the projected histograms (shown in side panels).

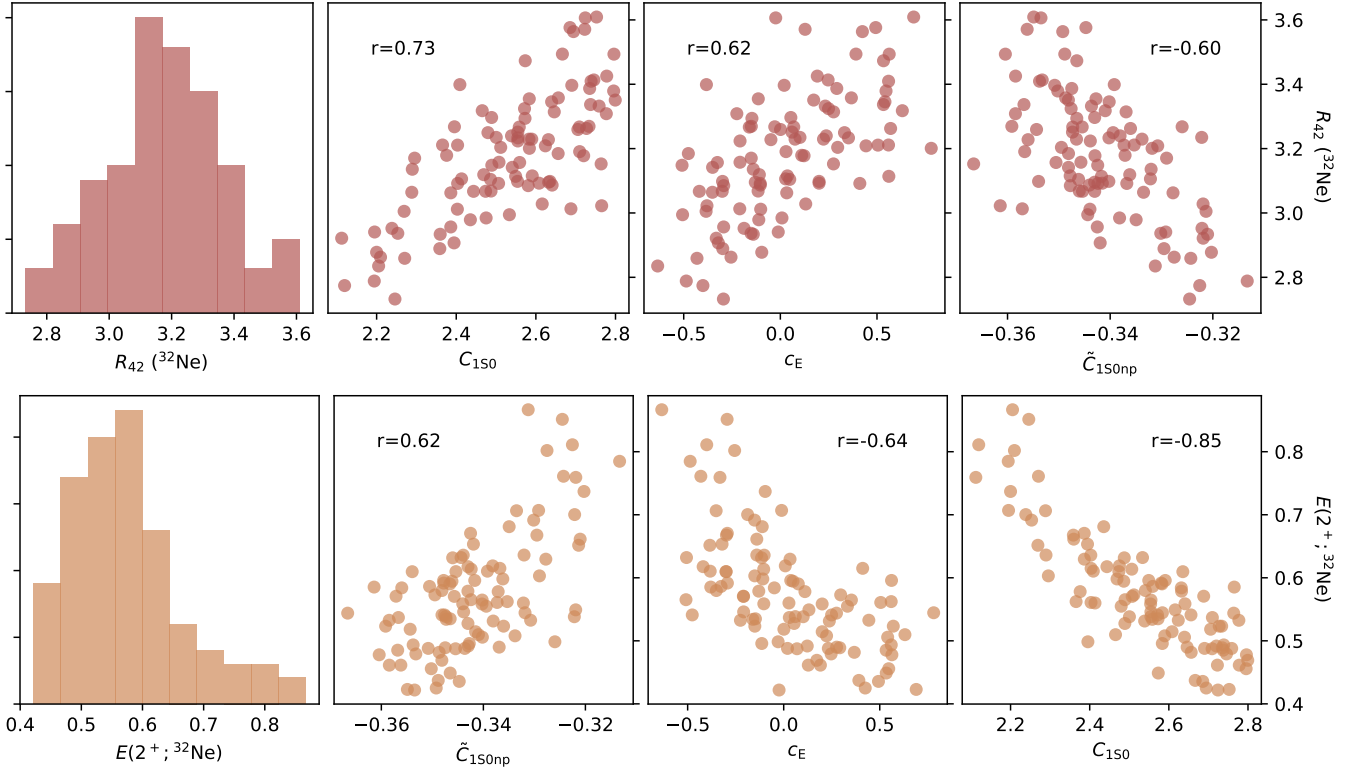


FIG. 8. Correlation between the low-energy constants of the Delta-full NNLO Hamiltonian and the observables  $R_{42}$  (upper row),  $E(2^+)$  (lower row) of  $^{32}\text{Ne}$ . The scatter plots include the  $\approx 100$  interaction samples from the history matching ensemble while the histograms show the distribution for the respective observable. The Pearson correlation coefficient,  $r$ , is extracted for the samples for each pair of variables. All other low-energy constants have correlation coefficients with an absolute magnitude smaller than 0.4 and are not shown.

- 
- [90] Hugh G. A. Burton. Generalized nonorthogonal matrix elements: Unifying wick's theorem and the slater–condon rules. *The Journal of Chemical Physics*, 154(14):144109, 2021.
- [91] A. Ekström, G. Baardsen, C. Forssén, G. Hagen, M. Hjorth-Jensen, G. R. Jansen, R. Machleidt, W. Nazarewicz, T. Papenbrock, J. Sarich, and S. M. Wild. Optimized chiral nucleon-nucleon interaction at next-to-next-to-leading order. *Phys. Rev. Lett.*, 110:192502, May 2013.
- [92] Jun-ichi Fujita and Hironari Miyazawa. Pion theory of three-body forces. *Prog. Theor. Phys.*, 17(3):360–365, 1957.
- [93] Nicholas D. Heller, Grigor H. Sargsyan, Kristina D. Launey, Calvin W. Johnson, Tomáš Dytrych, and Jerry P. Draayer. New insights into backbending in the symmetry-adapted framework, 2022.
- [94] Carlos A. Jiménez-Hoyos, Thomas M. Henderson, Takashi Tsuchimochi, and Gustavo E. Scuseria. Projected hartree–fock theory. *J. Chem. Phys.*, 136(16):164109, 2012.
- [95] Per-Olov Löwdin. Quantum theory of many-particle systems. ii. study of the ordinary hartree-fock approximation. *Phys. Rev.*, 97:1490–1508, Mar 1955.
- [96] Javier Rodriguez-Laguna, Luis Miguel Robledo, and Jorge Dukelsky. Efficient computation of matrix elements of generic slater determinants. *Phys. Rev. A*, 101:012105, Jan 2020.
- [97] Andrea Saltelli, Paola Annoni, Ivano Azzini, Francesca Campolongo, Marco Ratto, and Stefano Tarantola. Variance based sensitivity analysis of model output. design and estimator for the total sensitivity index. *Computer Physics Communications*, 181(2):259–270, 2010.